Iraqi Journal of Physics, 2022 *Vol. 20, No. 1, PP. 1-13*
DOI: 10.30723/ijp.v20i1.965 *P-ISSN: 2070-4003*
E-ISSN: 2664-5548

The Confinement Profile Effect on the Optical Properties in Different Inverse-shaped Single InGaN/GaN Quantum Wells

Redouane En-nadir[a,1*], Haddou El Ghazi[b,1,2], Walid Belaid [c,1,3], Hassan Abboudi[d,1], Fath allah Jabouti[e,1], Anouar Jorio[f,1], Izeddine Zorkani[g,1]
[1] LPS, FSDM, Sidi Mohammed Ben Abdellah University, Fes, Morocco
[2] SPME Group, ENSAM, Hassan II University, Casablanca, Morocco
[3] LPD, Microscopy Group, Faculty of Sciences, Selcuk University, Konya, Turkey
[b]E-mail: hadghazi@gmail.com, [c]E-mail:walid.belaid@usmba.ac.ma,
[d]E-mail:abboudihassan1@gmail.com, [e]E-mail:fathallahjabouti@gmail.com,
[f]E-mail:a_jorio@hotmail.com , [g]E-mail: izorkani@hotmail.com
[a*]Corresponding author: redouane.en-nadir@usmba.ac.ma

Abstract

In this work, the effects of size, and temperature on the linear and nonlinear optical properties in InGaN/GaN inverse parabolic and triangular quantum wells (IPQW and ITQW) for different concentrations at the well center were theoretically investigated. The indium concentrations at the barriers were fixed to be always x_{max} = 0.2. The energy levels and their associated wave functions are computed within the effective mass approximation. The expressions of optical properties are obtained analytically by using the compact density-matrix approach. The linear, nonlinear, and total absorption coefficients depending on the In concentrations at the well center are investigated as a function of the incident photon energy for different values of temperature and quantum wells size. The results show that the In concentrations, size and temperature have a significant effect on these optical properties. The positions of the resonance peaks of the absorption coefficients were blue-shifted under increasing indium compositions in the quantum wells (InGaN) and temperature while they were red-shifted with the increase in the thickness of the wells. Moreover, the amplitudes of the resonance peaks were enhanced under the increase of the In composition, the temperature, and the thickness of the quantum wells. The optical absorption in ITQW structure is slightly greater than that in IPQW one.

Article Info.

Keywords:
Optical properties, Intrasubband transitions, Inverse parabolic QW, Inverse triangular QW, In-compositions

Article history:
Received: Dec. 17, 2021
Accepted: Jan. 20, 2022
Published: Mar. 01,2022

1. Introduction

Due to their wide and direct bandgaps, group III-nitride semiconductor materials such as GaN, AlN, InN**,** and their associated alloys (AlGaN, InGaN) could crystalize in both wurtzite and zincblende at room temperature. These particular properties make them able to cover almost the entire electromagnetism spectrum from ultraviolet to infrared wavelength.

This is one of the reasons that make them become the suitable candidates of extremely intensive research in addition to their unique physical and thermodynamic properties and their high potential for short-wavelength electronic and optoelectronic devices application. These optoelectronic devices, especially absorbers and emitters such as light-emitting diodes (LEDs),

photodetectors, solar cells, and diodes lasers, can be active in the blue, green, and ultraviolet (UV) wavelengths [1-3].

The recent development in theoretical and experimental techniques, such as the metal-organic chemical vapor deposition (MOCVD) [4] and molecular-beam epitaxy (MBE) [5], the fabrication of low-dimensional systems have made it possible to grow nanoscale semiconductor heterostructures that are usually used to confine carriers (electrons, holes) and control their motion in pecific directions. Especially, in 1D (quantum wells) [6-8], 2D (quantum well wires) [9], and/or 3D (quantum dots) [10]. These types of heterostructures have attracted significant attention for both, their unusual physical properties compared to bulk crystals and their potential applications ina wide range of electronic and optoelectronic devices applications that are mentioned above.

The linear and third-order nonlinear optical properties in these heterostructures have been extremely investigated in recent years. Due to the existence of a strong quantum confinement effects are much stronger in low-dimensional systems compared to massive ones. The nonlinear optical properties of these structures have also led to exciting innovations in photodetection devices, such far-infraredared photo-detectors (FIPD), electro-optical modulators (EOM), infrared lasers (IRL), and all types of optical switches [11, 12].

Recently, several theoretical and experimental studies of linear and third-order nonlinear and total optical absorption coefficients have been presented based on single and multi-quantum wells (MQWs) with different shapes and geometries [13-17]. Zhang [18] reported the linear and nonlinear intrasubband transitions in a semi-parabolic QW with an external applied electric field. Keshavarz and Karami [19] have calculated the linear and nonlinear conduction intersubband optical absorption in asymmetric double semi-parabolic (SDQWs). Karami et al. [20] reported the linear and nonlinear intersubband optical absorption coefficients in asymmetric double semi-parabolic (QWs). Emine Ozturk and Sokmen [21] have investigated the effect of magnetic field on the nonlinear intersubband transitions in a parabolic and an inverse parabolic quantum well. The effects of applied electric and magnetic fields on the nonlinear optical properties of asymmetric GaAs/Ga1-xAlxAs double inverse parabolic quantum well were reported by Al et al. [22].

In one of our provious works [23], we theoreticaly examinated the effects of coupling, temperature and In-compositions on the optical properties of a double-coupled quantum wells (DQWs). However, in the recent study, a single QW structure with two different confinement potential profile (inverse parabolic and inverse triangular) was investigated in order to complete the previous work, compare, and optimize the optical properties in different situations. This work is organized as follows: introduction (Sec.1), theoretical framework (Sec.2), results and discussion (Sec.3) and conclusion in Sec.4.

2. Theory and models

2.1. Electronic states in QWs

Consider a single QW structure consisting of an unstrained $In_xGa_{1-x}N$ well with thickness *(l)* between two GaN barriers with thickness (L). The layers are grown on a GaN substrate and along the [1-100] direction (m-plan) which is the nonpolar plan in Wurtzite crystal structure. The origin is considered at the left corner of the QWs. In the absence of any external strenght, the Hamiltonian of the electron in the effective-mass approximation is given as follows:

$$\mathbf{H}=-\frac{\hbar^2}{2\mathbf{m}_e^*(T,x_c)}+\mathbf{V}_{\mathbf{P,T}}(l,T,x_c) \qquad (1)$$

where m_e^*, $\hbar$ are the electron effective-mass and the Planck constant, respectively.

The confinement potential for a single IPQW (V_P) and ITQW (V_T), have the following forms [23]:

$$V_P(z,l,x_c)=\begin{cases} V_0, & z<L \\ \frac{V_0}{\Omega}\left(1-\frac{4}{l^2}\left(z-L-\frac{l}{2}\right)^2\right), & L\leqslant z\leqslant L+l \\ V_0, & z>l+2L \end{cases} \quad (2)$$

And,

$$V_T(z,l,x_c)=\begin{cases} V_0, & z<L \\ \frac{V_0}{\Omega}\left(1-\left[-\frac{2}{l}\left(z-L-\frac{l}{2}\right)\right]\right), & L\leqslant z<L+\frac{l}{2} \\ \frac{V_0}{\Omega}\left(1-\left[\frac{2}{l}\left(z-L-\frac{l}{2}\right)\right]\right), & L+\frac{l}{2}\leqslant z\leqslant L+l \\ V_0, & z>l+2L \end{cases} \quad (3)$$

where $V_0=0.7\times\left[E_g^{GaN}-E_g^{InGaN}(x_c)\right]$ is the band discontinuity, at room temperature and for $x_{max}=x_c=0.2$ and $l=L=2$, is equal to (810.73 *meV*). $\frac{V_0}{\Omega}$ is the maximum value of the potential at the center of IPQW and ITQW, and l is the width of the single IPQW and ITQW. $\Omega=\frac{x_{max}}{x_c}(x_{max})$ is the constant indium compositions (*In*) at the barriers (GaN), x_c the *In* compositions at the well region ($In_xGa_{1-x}N$)).

According to Gazzah et al. [24, 25], the band-gaps energy, the effective-mass and the dielectric constant of the binaries InN and GaN as a function of temperature are expressed respectively by:

$$E_g^{GaN,InN}(T)=E_g^{GaN,InN}(T=0K)-\frac{\alpha^{GaN,InN}\times 10^{-3}T^2}{\beta^{GaN,InN}+T} \quad (4)$$

$$\frac{m_0}{m^*_{GaN,InN}(T)}=1+\frac{C^{GaN,InN}}{E_g^{GaN,InN}(T)} \quad (5)$$

$$\varepsilon_r^{GaN}(T)=\varepsilon_r^{GaN}(T=300K)e^{(T-300)10^{-4}} \quad (6)$$

$$\varepsilon_r^{InGaN}(T)=\varepsilon_r^{GaN}(T)+6.4x_c \quad (7)$$

To obtain the ground (1S-state), second-excited state (2P-state) and their associated energy levels of the Hamiltonian (1), the finite element method (FEM) was used taking into account the continuty of electron effective-mass as well as the dielectric constant at the interfaces between the barriers (GaN) and the well (InGaN). The boundary conditions are given by the following equation [26],

$$\left[\vec{n}\cdot\vec{\nabla}\left(\frac{\psi}{m^*_{e,b}}\right)\right]_{Barriers}=\left[\vec{n}\cdot\vec{\nabla}\left(\frac{\psi}{m^*_{e,w}}\right)\right]_{QW} \quad (8)$$

The mesh-grid of 3N+1 point is considered for both layers (Barriers/wells). We provided A specific discretization step for each layer was provided. For the well, the step is h_w (=l /N) whereas for the barrier regions it is given as h_b (=L/N). Moreover, for 0<i<N (=50 pts), the mesh's nodes of the investigated structures are given respectively as fellows, left barrier zi (=i*hb), in the well region zi (=L+i*hb) and in the right barrier region is given as zi(=L+ l +i*hb).

The derivatives electron wave functions are given by the following expressions:

$$\frac{\partial^2\psi(z)}{\partial z^2}\Big)_{z_i} = \frac{\psi_{i+1}-2\psi_i+\psi_{i-1}}{(z_{i+1}-z_i)^2} \quad \textbf{(9.a)}$$

$$\frac{\partial\psi(z)}{\partial z}\Big)_{z_i} = \frac{\psi_{i+1}-\psi_i}{z_{i+1}-z_i} \quad \textbf{(9.b)}$$

The physical parameters that have been used in our calculations are listed in Table 1 [24-27].

Table 1: The physical characteristics of GaN and InN.

Parameters	GaN	InN
E_g^i(T=0)	3.29	0.72
m_i^*(T=0) (m_0)	0.20	0.11
ε_i^* (ε_0)	9.6	10.5
α	0.909	0.24
β	830	624
C	14.7	15.5

2.2. Optical properties

The analytical expressions of the linear and nonlinear optical absorption coefficients in low-dimensional systems can be obtained within the framework of the density matrix approach and the perturbation expansion method. So that, the corresponding coefficients can be written, within a two-level system approximation, as follows [28, 29]:

$$\alpha^1(\omega)=\hbar\omega\sqrt{\frac{\mu}{\varepsilon_r^*\varepsilon_0}}\frac{\Gamma_{if}|M_{fi}|^2\rho}{(E_{fi}-\hbar\omega)^2+(\hbar\Gamma_{if})^2} \quad \textbf{(10)}$$

$$\alpha^3(\omega,I)=-\sqrt{\frac{\mu}{\varepsilon_r^*}}\left(\frac{I}{2n_r^*\varepsilon_0 c}\right)\frac{4\Gamma_{if}|M_{fi}|^4\rho\,\hbar\omega}{[(E_{fi}-\hbar\omega)^2+(\hbar\Gamma_{if})^2]^2}\left[1-\frac{|M_{ff}-M_{ii}|^2}{4|M_{ff}|^2}\times\frac{3E_{fi}^2-4\hbar\omega E_{fi}+(\hbar\omega)^2-(\hbar\Gamma_{if})^2}{E_{fi}^2-(\hbar\Gamma_{if})^2}\right] \quad \textbf{(11)}$$

Therefore, the total OAC is given as the sum of the linear and third-order nonlinear optical contributions as follows [27]:

$$\alpha^T(\omega,I)=\alpha^1(\omega)+\alpha^3(\omega,I) \quad \textbf{(12)}$$

The diagonal dipole matrix element and the transition energy that satisfy the selection rule between two different implied states ($\Delta l=\pm 1$) can be defined respectively by Eq. (13.a, 13.b):

$$M_{if}=\langle\psi|ez|\psi\rangle \quad \textbf{(13.a)}$$

$$\Delta E_{fi}=E_f-E_i \quad \textbf{(13.b)}$$

The electron density in the quantum well region (InGaN)= $\rho=2\times10^{26}$ m^{-1}, the incident pump intensity $I=3\times10^{10}$ W/m^2, and the relaxation time between allowed electronic states $\Gamma_{fi}=\frac{1}{\tau_{fi}}$ ($=5\times10^{12}$ s^{-1}).

3. Results and discussion

In this work, the effective units only were adopted in order to simplify the calculations. Indeed, the effective Rydberg $R^*=\frac{m_b^* e^4}{2\hbar^2\varepsilon_0^2}$ as the unit of energy as well as the effective Bohr radius

$a^* = \frac{\varepsilon_0 \hbar^2}{m_b^* e^2}$ as the unit of length were considered. At room temperature (T=300K) and for $x_{max}=x_c=0.2$ (100%); $l = L = 2$, these effective units are equal to 27.55 *meV* and 2.70 *nm*, respectively.

3.1. Energy levels in IPQW/ITQW

The confinement potential profile as well as the the square of the three low-laying electron wave-functions as a function of growth direction for three different values of Ω and x_c are depicted in Fig.1. It is important to notice that, in the case of $x_c=0.05$ corresponding to Ω =4, the QWs became practically a quasi-square quantum well for both IPQW and ITQW whereas when $x_c = x_{max} = 0.2$ corresponding to Ω =1, the studied structures became practically a quasi-W-shape quantum well (W-shape). However, if the square of three first wave functions of both IPQW and ITQWwere compared, it is observed that they changed under the change in Ω. The smallest Ω is the localized density of probability in the corners of the QWs.

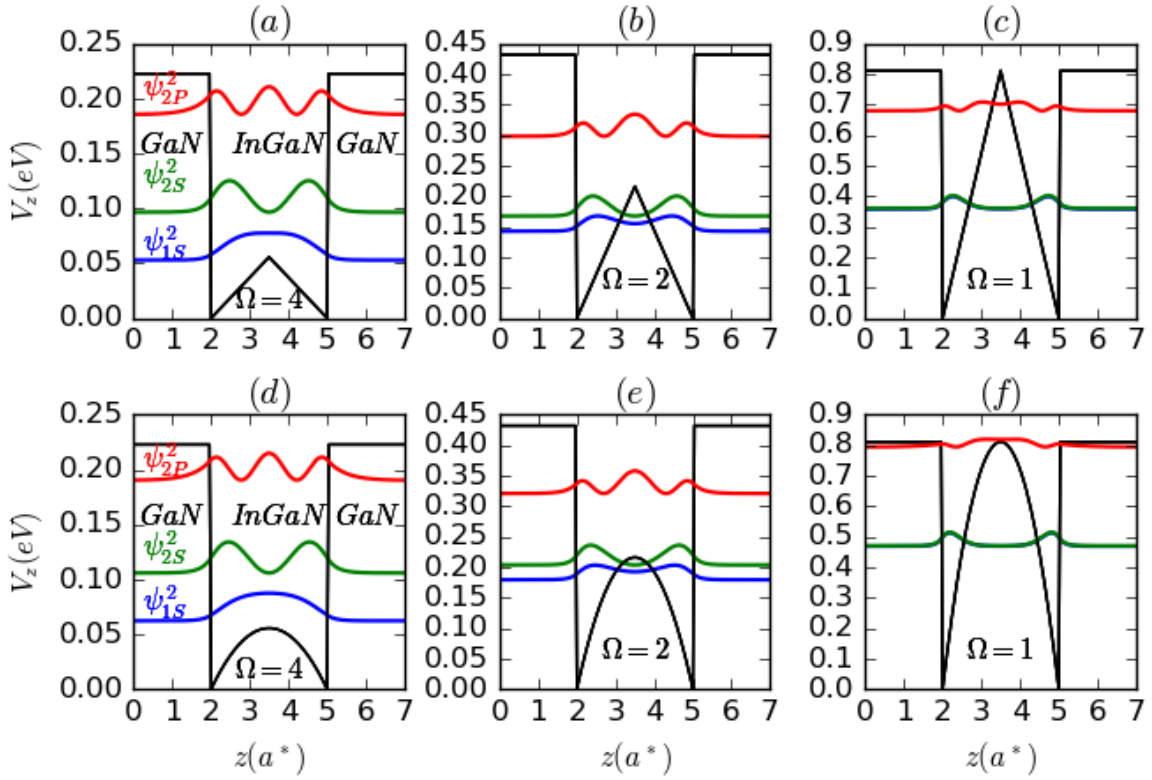

Figure 1: The confinement potential profile as well as the square of the three low-laying electron wave-functions versus z-axis for three different values of Ω(x_c)=4(2,1) for two QW's shapes ITQW and IPQW.

This is due to the increase of the quantum confinement inside the QWs with the diminishing of Ω (increase in x_c). It also noticed that the decrease of Ω induced an augmentation of the energy levels in both structures IPQW and ITQW. In addition, the above effects are more noticeable in the IPQW than in the ITQW. This can be explained by the fact that the increase in Ω induces an increase in the quantum confinement in the IPQW structure more than in ITQW structure. Consequently, these results have a significant importance in studying the change in the optical properties under the above-mentioned parameters of such nanostructure.

The change in the energy levels as a function of the well width, temperature and Ω for both IPQW and ITQW are depicted in Fig.1. According to this figure, for a fixed barriers width (L=2), it is obvious that the change of those parameters had a remarkable influence on the electronic energy levels in both structures ITQW (A) and/or IPQW (B). It can be seen that the energy levels increased to reach a maximum at a critical value of well width about (l=1) and then decreased until a stable regime was reached towards the region where there was a low confinement for wide QWs (l>5) for both considered structures as it expected. The physical reason is that, for QW's with around a*(l=1), the quantum confinement becomes maximal and the particle becomes sensitive to the barriers material (GaN) and then starts to penetrate in the barrier region (GaN) which translates to diminishes in the particle energy in both structures ITQW and IPQW. Therefore, the increase of Ω (decrease in x_c) leads to a drop of about 100 *meV* of the energy levels towards lower energies for both considered structures. This can be explained by the fact that, the decrease in Ω (increase in *xc* in the QW regions) rises the quantum confinement inside the QWs which induces the enhancement in the energy levels as expected. It is also noticed that these energy levels decreased with the increase in temperature, which can be explained by the thermal concept that when the temperature increases, the electron's kinetic energy increases and then their proper energy levels drop.

The variation of the difference of energy between allowed electron's energy levels in the conduction band versus the well width as well as temperature for a fixed barrier's size (L=2) for both investigated structures ITQW and IPQW are presented in Fig.2 (a and B). From this figure, it can clearly be seen that, the energy shift between electron levels (right panel) depends on the well size, also temperature varies in the same way as energy levels separately. For both studied structures IPQW (B) and ITQW (A), ΔE_{fi} rose to reach a maximal value at about 300 meV for ITQW (A), however, it was about 250 meV for IPQW (B) for an identic critical value of the well size about a* and then decreased to reach a minimal value around 100 mV for both structures ITQW (A) and IPQW (B). Therefore, it was noticed that ΔE_{fi} of ITQW (A) structure was always greater than that of IPQW (B) for all values of well size and temperature, which explains the behavior observed in the same Fig.3 (a). The physical reasons behind this are the same devoted to explain the above results.

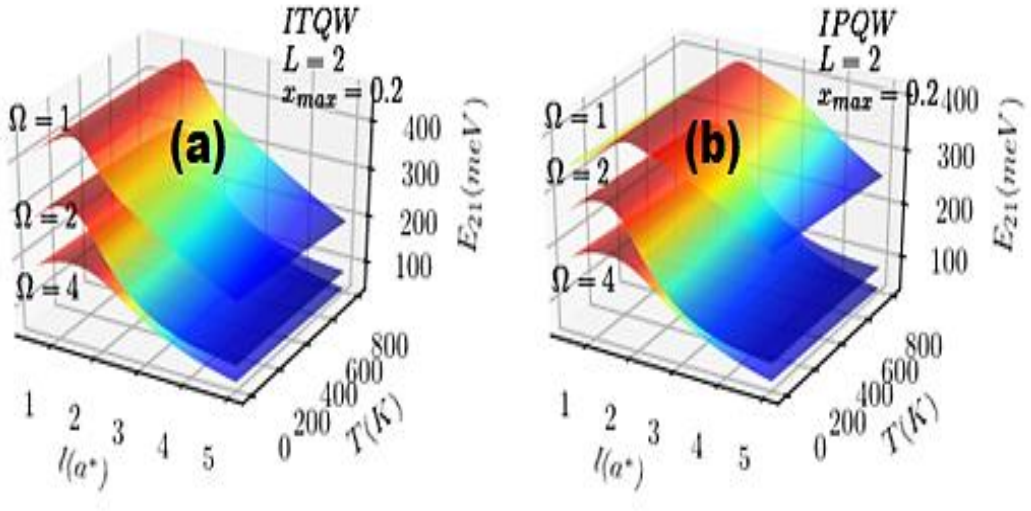

Figure 2: The variation of the three low-lying energy levels in both ITQW (a) and IPQW (b) versus the well width (x-axis) and temperature (y-axis) with a fixed barrier width (L=2) and x_{max}=0.2 for three different values of Ω=4(2,1).

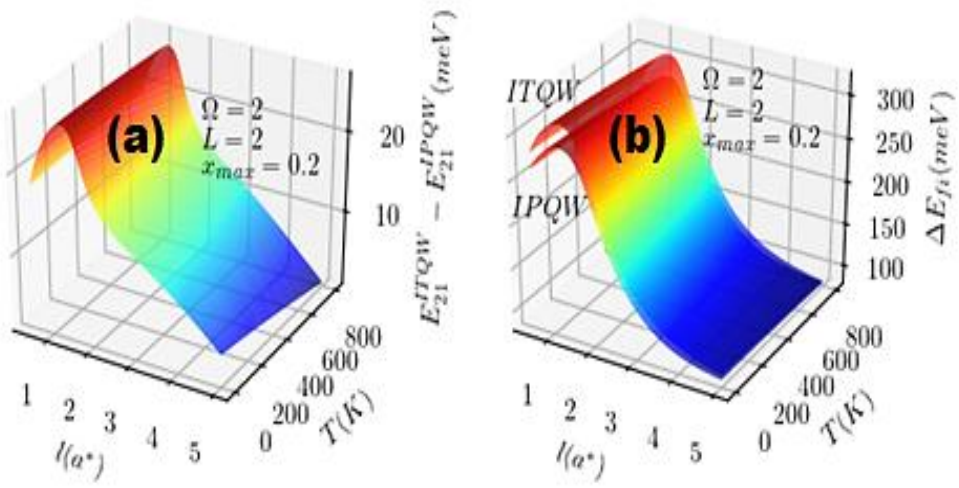

Figure 3: The variation of the difference of energy between both of them (ITQW and IPQW) (a) and that of them separately (B) versus the well width (x-axis) and temperature (y-axis) with a fixed barrier width (L=2) and x_{max}=0.2 and Ω=2.

3.2. The transition dipole moment in IPQW and ITQW

As for the behavior of the transition dipole moment under the impact of the discussed parameters above. First, it is crucial to mention that the transition dipole moment between two allowed quantum states (also called dipole matrix element or M_{fi}) is one of the main parameters in the linear and nonlinear optical coefficients. So that, it is necessary to thoroughly study this parameter under the effect of different perturbations such as size, temperature, and internal compositions. According to Fig.4 (b), for a fixed barrier's size (L=2), the square of M_{fi} increased with increasing either temperature or the well's size for both considered structures, ITQW and IPQW, while it was higher for ITQW than that in IPQW. According to Eq. (12.a), it is clear that this quantity depends on distance.

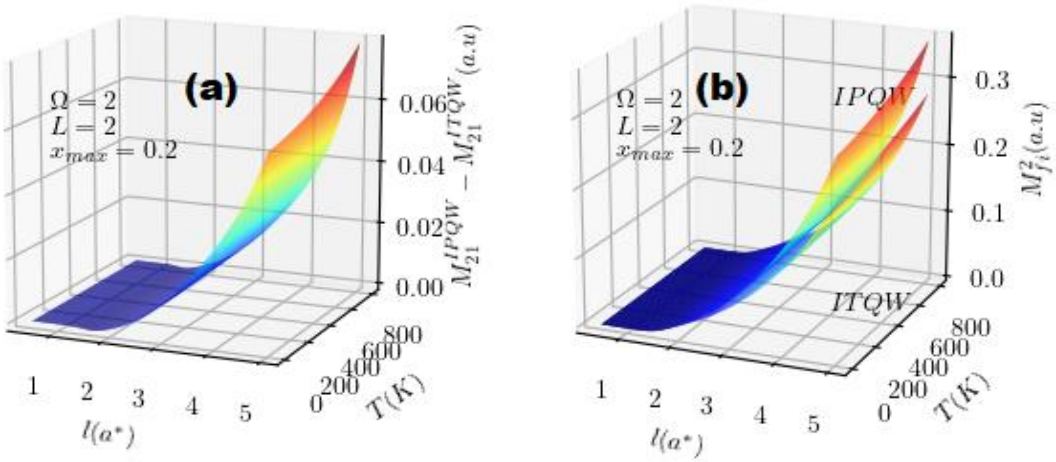

Figure 4: The variation of the electric dipole transition moment between both of them (ITQW and IPQW) (a) and that of them separately (b) versus the well width (x-axis) and temperature (y-axis) with a fixed barrier width (L=2) and x_{max}=0.2 and Ω=2.

Thus, the increase of the square of M_{fi} is due to the increase in the width of the well while the increase caused by the increase in temperature can be explained by the fact that with the increase of the temperature, the particle acts as it is less bounded, which results in the increase in M_{fi}. It is also noticed that the square of M_{fi} in IPQW was always greater than that of ITQW for all values of temperature and well's size. These results explain the behavior noticed in the same Figure (a) in which the difference of the square of M_{fi} of both considered structures increased with the increase in temperature and size as well. Moreover, Fig.5 (a and b) shows the variation of the square of M_{21} of both structures IPQW (A) and ITQW (B) as a function of compositions (x-axis) as well as temperature (y-axis). According to this figure, the square of M_{21} of both structures IPQW (A) increased to reach a saturation regime then decreased in a critical value of composition about the chosen maximum value (0.2). Since, when the indium composition increases in the well (InGaN), the material changes the direct band-gap character into indirect, which induces that drop in M_{21}, whereas this is not shown for ITQW (b) structure because in this structure, the confinement is less than that of IPQW (a).

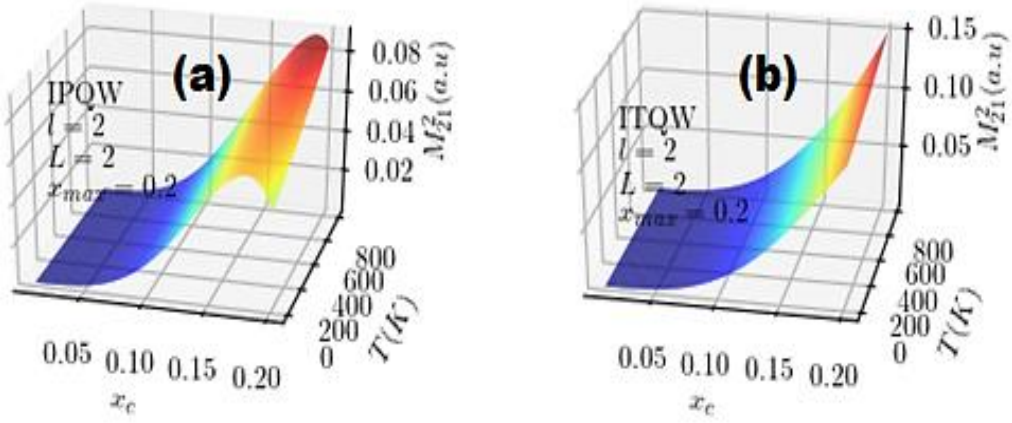

Figure 5: The variation of the electric dipole transition moment in both ITQW (a) and IPQW (b) and versus the In-compositions (x-axis) and temperature (y-axis) with a fixed barrier/well width (L=l=2) and x_{max}=0.2.

3.3. The optical properties in IPQW and ITQW

For a physical interpretation and understanding of the optical properties results, it is very important to take into account some of the OACs key qualities, which were listed above. However, the absorption spectra positions of OACs was obtained at $\hbar\omega=\sqrt{E_{21}^2+(\hbar\Gamma_{21})^2}$ and its amplitude's maximum was estimated by $|M_{21}|^2/\sqrt{E_{21}^2+(\hbar\Gamma_{21})^2}$. Since the rate $\frac{|M_{ff}-M_{ii}|^2}{4|M_{ff}|^2}$ is insensitive to narrow QW and disappears quickly, that leads to a minor contribution in the second term in parentheses of the nonlinear optical absorption coefficient (Eq. (11)). Otherwise, the nonlinear contribution reaches its maximum approximately, at the same value as that of the linear one. However, the maximum amplitude is governed by $|M_{21}|^4/\sqrt{\left(E_{21}^2+(\hbar\Gamma_{21})^2\right)^{3/2}}$. Assuming that, $\hbar\Gamma fi \ll Efi$ is true for all scenarios associated to the indium compositions inside the QW (InGaN), the size of the structure and the temperature, the OACs must be maximal around the difference of energy between the involved quantum states $\hbar\omega_{21}\approx E_{21}$. The maximum of the total OAC amplitude, on the other hand, is given by two

parameters that act in opposite tendencies, $|M_{21}|^2/E_{21}$ for the linear contribution, while it is $|M_{21}|^4/E_{21}^3$ for the nonlinear one. The above-mentioned characteristics of the transition energy differences as well as the electric transition dipole moment provide the information required for the best physical explanation of the behaviors of the linear, non-linear and total optical absorption coefficients. To show the influence of those physical quantities under the effect of the In-compositions, temperature and size's width, we depicted their impact on linear, non-linear and total optical absorption coefficients (OACs) versus the incident photon energy (R*), were shown in Figs.6-8.

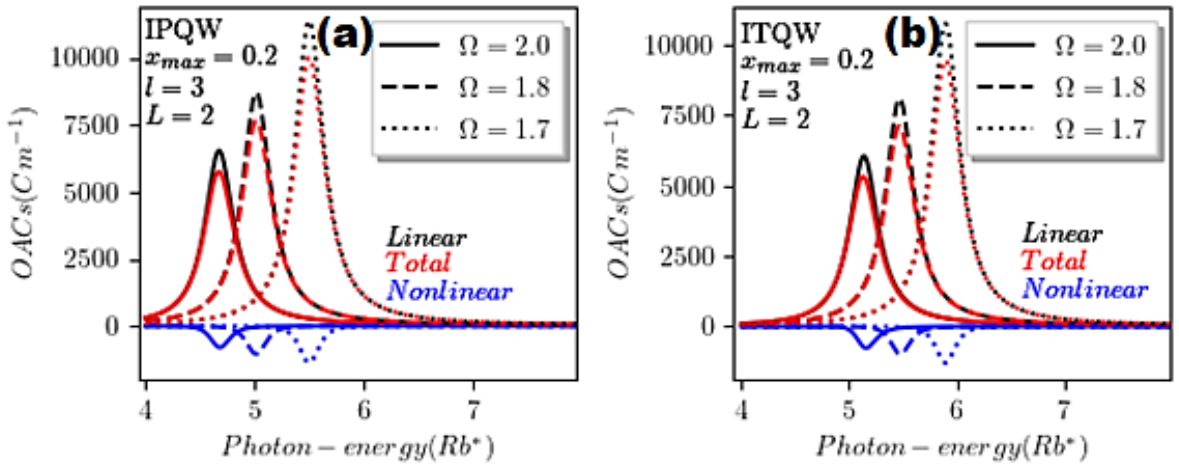

Figure 6: The OACs change versus incident photon energy (R*) with fixed barriers/well widths (L=2; l=3) and x_{max}=0.2 for three different values of Ω=2(1.8; 1.7) considering two potential shapes IPQW (a) and ITQW (b).

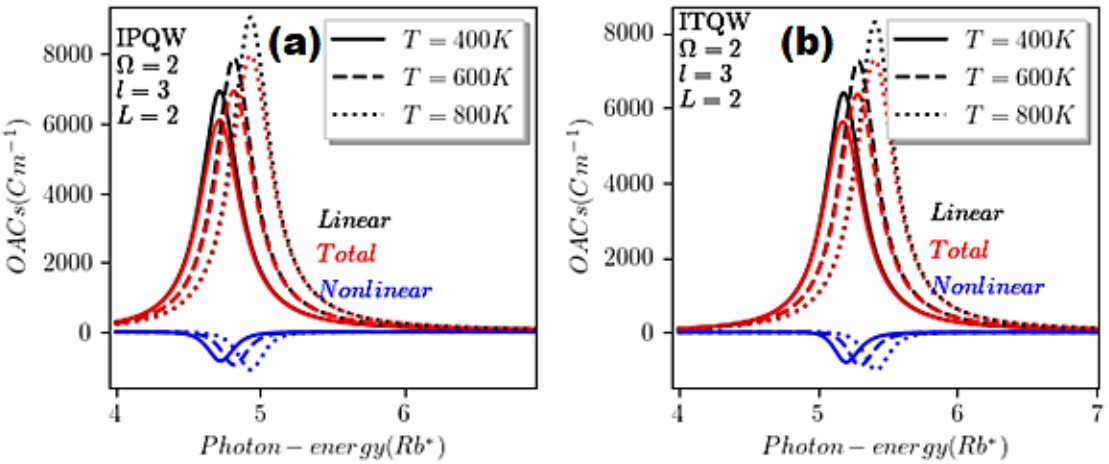

Figure 7: The OACs change versus incident photon energy (R*) with fixed barriers/well widths (L=2; l=3) and x_{max}=0.2 (Ω=2) for three different values of temperature T=400K (600K; 800K) considering two potential shapes IPQW (a) and ITQW (b).

From the above-mentioned figures, it can clearly be seen that the resonance peak as well as their corresponding maximums has been changed for the two studied structures IPQW and ITQW by the variation of the compositions in the QW, the temperature and size. On the one hand, the reduction of Ω (2→1.7) generated a shift of the resonance peak of OACs towards high energies accompanied by a significant improvement of their associated amplitudes for both structures (ITQW and IPQW) as it expected, which is in good conformity with the results discussed in Figs. 3-5. On the other hand, a similar behavior is observed in Fig.7 with increasing

the temperature. The physical reasons were discussed at the beginning of this section. However, in Fig.8, the resonance peak is shifted towards lower energy with increasing the well's width (2→2.2a*), which is expected, and the related amplitudes have been enhanced as well. This is in great accordance with the results discussed earlier for either ITQW or IPQW.

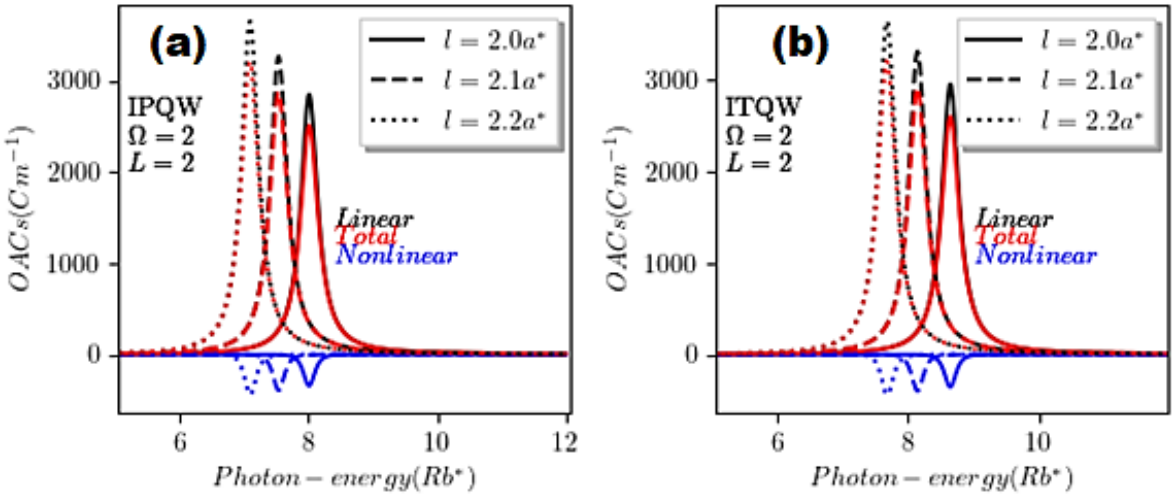

Figure 8: The OACs change versus incident photon energy (R*) with fixed barriers widths (L=2) and x_{max}=0.2 (Ω=2) at room temperature (T==300K) for three different values of the well width l=2(2.1; 2.2) considering two potential shapes IPQW (a) and ITQW (b).

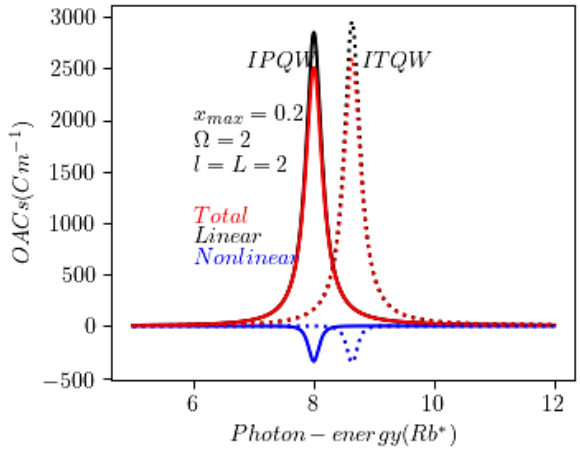

Figure 9: The OACs change of both IPQW and ITQW versus incident photon energy (R*) with fixed barriers/well widths (L=l=2) and x_{max}=0.2 (Ω=2) at room temperature (T=300K).

To compare the difference between the OACs in both investigated structures ITQW and IPQW, their results were depicted in the same plot (Fig.9). According to this figure, changing IPQW structure by ITQW, induces a blue shift of the resonance peak of the OACs as well as improving their corresponding amplitudes. This is in good accordance with the above-discussed results for both energy and dipole matrix element. This is due to that fact that the quantum confinement into the ITQW structure is slightly greater than that in IPQW structure, which leads to the last result.

Our study was compared to previous literature studies and showed good agreement. Our study can be confirmed by the study reported by Ungan et al. [30] on the linear and nonlinear optical properties in GaAs/AlGaAs inverse parabolic quantum well and by that reported

recently by Ozturk [31] to compare asymmetric double parabolic-inversed and parabolic quantum wells for one optical transition.

4. Conclusions

In this work, the effects of confinement profile, well thickness and temperature on the linear, nonlinear and total optical absorption coefficients (OACs) were theoretically reported. The results showed that these parameters have a great effect on the linear and non-linear optical properties of quantum wells made out of InGaN/GaN. Moreover, with increasing In-composition and temperature, a blue-shift resulted and its amplitude of OACs for both structures ITQW and IPQW was improved, while a red-shift accompanied with improvement in the amplitudes of OACs for both structures ITQW and IPQW was obtained with increasing the well width. Moreover, a blue-shift associated with an improvement of the OAC's maximums was observed with changing the confinement potential profile.

Acknowledgements

The author would like to thanks all the co-authors for sharing so-called insight and comments.

Conflict of interest

The authors declare that they have no known competing financial interests or personal relationships that could have appeared to influence the work reported in this paper.

References

1. Acharya A.R., *Group III–nitride semiconductors: preeminent materials for modern electronic and optoelectronic applications.* Himalayan Physics, 2014. **5**: pp. 22-26.
2. Edward T.Y., *III-V nitride semiconductors: Applications and devices*. 2002.
3. Beeler M ,.Trichas E., and Monroy E., *III-nitride semiconductors for intersubband optoelectronics: a review.* Semiconductor Science Technology, 2013. **28**(7): pp. 1-26.
4. Wang J., Nozakib M., Ishikawa Y., Hao M., Morishima Y., Wang T., Naoi Y., and Sakai S., *Fabrication of nanoscale structures of InGaN by MOCVD lateral overgrowth.* Journal of crystal growth, 1999. **197**(1-2): pp. 48-53.
5. Lee S., Stintz A., and Brueck S., *Nanoscale limited area growth of InAs islands on GaAs (001) by molecular beam epitaxy.* Journal of applied physics, 2002. **91**(5): pp. 3282-3288.
6. hi Z., Yuan J., Zhang S., Liu Y., and Wang Y., *Simultaneous dual-functioning InGaN/GaN multiple-quantum-well diode for transferrable optoelectronics.* Optical Materials, 2017. **72**: pp. 20-24.
7. Chen Y., Maharjan N., Liu Z., Nakarmi M., Chaldyshev V., Kundelev E., Poddubny A., Vasil'ev A., Yagovkina M., and Shakya N., *Resonant optical properties of AlGaAs/GaAs multiple-quantum-well based Bragg structure at the second quantum state.* Journal of Applied Physics, 2017. **121**(10): pp. 1-9.
8. Islam A.B.M.H., Shim J.-I., and Shin D.-S., *Optoelectronic performance variations in InGaN/GaN multiple-quantum-well light-emitting diodes: effects of potential fluctuation.* Materials 2018. **11**(5): pp. 1-11.
9. Goni A., Pfeiffer L., West K., Pinczuk A., Baranger H., and Stormer H., *Observation of quantum wire formation at intersecting quantum wells.* Applied physics letters, 1992. **61**(16): pp. 1956-1958.
10. Bera D., Qian L., Tseng T.-K., and Holloway P.H., *Quantum dots and their multimodal applications: a review.* Materials, 2010. **3**(4): pp. 2260-2345.

11. Karunasiri R., Mii Y., and Wang K.L., *Tunable infrared modulator and switch using Stark shift in step quantum wells.* IEEE electron device letters, 1990. **11**(5): pp. 227-229.
12. Zhao L.-X., Yu Z.-G., Sun B., Zhu S.-C., An P.-B., Yang C., Liu L., Wang J.-X., and Li J.-M., *Progress and prospects of GaN-based LEDs using nanostructures.* Chinese Physics B, 2015. **24**(6): pp. 1-12.
13. Yesilgul U., Ungan F., Al E.B., Kasapoglu E., Sari H., Sökmen I.J.O., and Electronics Q., *Effects of magnetic field, hydrostatic pressure and temperature on the nonlinear optical properties in symmetric double semi-V-shaped quantum well.* Optical Quantum Electronics, 2016. **48**(12): pp. 1-11.
14. Abdelwahab I., *Linear and Nonlinear Optical Studies of Two-dimensional Perovskites*, Thesis, 2019.
15. Ozturk O., Ozturk E., and Elagoz S., *Linear and nonlinear optical absorption coefficient and electronic features of triple GaAlAs/GaAs and GaInAs/GaAs quantum wells depending on barrier widths.* Optik, 2019. **18**0: pp. 394-405.
16. Hasanirokh K., Asgari A., and Rokhi M.M., *Theoretical study on nonlinear optical properties of CdS/ZnS spherical quantum dots.* Optik, 2019. **188**: pp. 99-103.
17. El Aouami A., Bikerouin M., Feddi K., Aghoutane N., El-Yadri M., Feddi E., Dujardin F., Radu A., Restrepo R., and Vinasco J., *Linear and nonlinear optical properties of a single dopant in GaN conical quantum dot with spherical cap.* Philosophical Magazine, 2020. **100**(19): pp. 2503-2523.
18. Zhang L., *Electric field effect on the linear and nonlinear intersubband refractive index changes in asymmetrical semiparabolic and symmetrical parabolic quantum wells.* Superlattices Microstructures, 2005. **37**(4): pp. 261-272.
19. Keshavarz A. and Karimi M., *Linear and nonlinear intersubband optical absorption in symmetric double semi-parabolic quantum wells.* Physics Letters A, 2010. **374**(26): pp. 2675-2680.
20. Karimi M., Keshavarz A., and Poostforush A., *Linear and nonlinear intersubband optical absorption and refractive index changes of asymmetric double semi-parabolic quantum wells.* Superlattices Microstructures, 2011. **49**(4): pp. 441-452.
21. Ozturk E. and Sokmen I., *Nonlinear intersubband transitions in a parabolic and an inverse parabolic quantum well under applied magnetic field.* Journal of luminescence, 2014. **145**: pp. 387-392.
22. Al E., Ungan F., Yesilgul U., Kasapoglu E., Sari H., and Sökmen I., *Effects of applied electric and magnetic fields on the nonlinear optical properties of asymmetric GaAs/Ga1-xAlxAs double inverse parabolic quantum well.* Optical Materials, 2015. **47**: pp. 1-6.
23. En-nadir R., El Ghazi H., Belaid W., Jorio A., and Zorkani I., *Intraconduction band-related optical absorption in coupled (In, Ga) N/GaN double parabolic quantum wells under temperature, coupling and composition effects.* Results in Optics, 2021. **5**: pp. 1-7.
24. Gazzah M.H., Chouchen B., Fargi A., and Belmabrouk H., *Electro-thermal modeling for InxGa1-xN/GaN based quantum well heterostructures.* Materials Science in Semiconductor Processing, 2019. **93**: pp. 231-237.
25. Abboudi H., El Ghazi H., Benhaddou F., En-Nadir R., Jorio A., and Zorkani I., *Temperature-related photovoltaic characteristics of (In, Ga) N single intermediate band quantum well solar cells for different shapes.* Physica B: Condensed Matter, 2021: pp. 413495.
26. Deyasi A., Bhattacharyya S., and Das N., *Computation of intersubband transition energy in normal and inverted core–shell quantum dots using finite difference technique.* Superlattices Microstructures, 2013. **60**: pp. 414-425.
27. En-nadir R., El Ghazi H., Belaid W., Jorio A., Zorkani I., and Kiliç H.Ş., *Ground and first five low-lying excited states related optical absorption in In. 1Ga. 9N/GaN double quantum*

wells: Temperature and coupling impacts. Solid State Communications, 2021. **338**: pp. 1-8.
28. Almansour S., *Numerical simulation of the effects of electric and magnetic fields on the optical absorption in a parabolic quantum well.* Journal of the Korean Physical Society, 2019. **75**(10): pp.810-806 .
29. Dakhlaoui H., Ungan F., Martínez-Orozco J.C., and Mora-Ramos M.E., *Theoretical investigation of linear and nonlinear optical properties in an heterostructure based on triple parabolic barriers: Effects of external fields.* Physica B: Condensed Matter, 2021. **607**: pp. 1-7.
30. Ungan F., Martínez-Orozco J.C., Restrepo R., Mora-Ramos M.E., Kasapoglu E., and Duque C.A., *Nonlinear optical rectification and second-harmonic generation in a semi-parabolic quantum well under intense laser field: effects of electric and magnetic fields.* Superlattices Microstructures, 2015. **81**: pp. 26-33.
31. Ozturk E., *Comparison of asymmetric double parabolic-inversed parabolic quantum wells for linear optical (1–2) transition.* Optik, 2017. **139**: pp. 256-264.

تأثير شكل البئر الكمومي للحصر درجة الحرارة وتركيز الإنديوم على الخصائص البصرية في الآبار الكمومية المستخدمة في أجهزة الليزر وأجهزة الكشف الضوئية

رضوان الناظر[1]*، حدو الغازي[2،1]، وليد بلعيد[3،1]، حسن العبودي[1]، فتح الله الجابوتي[1]، أنور جوريو[1]، عزالدين زرقاني[1]
[1]قسم الفيزياء، كلية العلوم، جامعة سيدي محمد بن عبد الله، فاس، المغرب
[2]المدرسة العليا للفنون والحرف، جامعة الحسن الثاني، الدار البيضاء، المغرب
[3]قسم الفيزياء، كلية العلوم، جامعة سلجوق، قونية، تركيا

الخلاصة

في هذه المقالة، درسنا نظريًا تأثيرات الحجم وتركيب الإنديوم ودرجة الحرارة على الخصائص البصرية الخطية وغير الخطية في الآبار الكمومية المقلوبة لتركيزات مختلفة من الإنديوم في مركز البئر الكمومي. يتم حساب مستويات الطاقة والوظائف الموجية المرتبطة بها في إطار نظرية الكتلة الفعالة. يتم الحصول على التعبيرات التحليلية للخصائص البصرية تحليليًا باستخدام نهج مصفوفة الكثافة المدمجة. معاملات الامتصاص الخطية وغير الخطية والإجمالية كدالة لطاقة الفوتون الساقط تحت تأثير تركيزات الإنديوم في مركز الآبار الكمومية المقلوبة ودرجة الحرارة وحجم البئر الكمي. أظهرت النتائج أن تركيزات الإنديوم وحجم الآبار الكمومية ودرجة الحرارة لها تأثير معنوي على الخواص البصرية الخطية وغير الخطية للآبار الكمومية المقلوبة. لاحظنا أن مواضع قمم الرنين لمعاملات الامتصاص قد تحولت نحو منطقة الأطوال الموجية الزرقاء تحت زيادة تركيبات الإنديوم في الآبار الكمومية (InGaN) ودرجة الحرارة بينما تم إزاحتها نحو منطقة الطول الموجي الأحمر مع زيادة سمك البئر. علاوة على ذلك، تمت زيادة الحد الأقصى لقمم الرنين مع زيادة تركيبة الإنديوم ودرجة حرارة وسمك الآبار الكمومية أيضًا.